APL Materials

Charge injection and trapping at perovskite interfaces with organic hole transporting materials of different ionization energies

Cite as: APL Mater. **7**, 041115 (2019); https://doi.org/10.1063/1.5086692
Submitted: 21 December 2018 . Accepted: 20 March 2019 . Published Online: 16 April 2019

Nikolaos Droseros, Benedikt Dänekamp, Demetra Tsokkou, Pablo P. Boix, and Natalie Banerji

Charge injection and trapping at perovskite interfaces with organic hole transporting materials of different ionization energies

Cite as: APL Mater. 7, 041115 (2019); doi: 10.1063/1.5086692
Submitted: 21 December 2018 • Accepted: 20 March 2019 •
Published Online: 16 April 2019

Nikolaos Droseros,[1] Benedikt Dänekamp,[2] Demetra Tsokkou,[1] Pablo P. Boix,[2] and Natalie Banerji[1,a)]

AFFILIATIONS

[1] Department of Chemistry and Biochemistry, University of Bern, Freiestrasse 3, CH-3012 Bern, Switzerland
[2] Instituto de Ciencia Molecular, Universidad de Valencia, C/ Catedrático J. Beltrán 2, 46980 Paterna, Valencia, Spain

Note: This paper is part of the special topic on Perovskite Semiconductors for Next Generation Optoelectronic Applications.
[a)] **Author to whom correspondence should be addressed:** natalie.banerji@dcb.unibe.ch

ABSTRACT

The extraction of photogenerated holes from $CH_3NH_3PbI_3$ is crucial in perovskite solar cells. Understanding the main parameters that influence this process is essential to design materials and devices with improved efficiency. A series of vacuum deposited hole transporting materials (HTMs) of different ionization energies, used in efficient photovoltaic devices, are studied here by means of femtosecond transient absorption spectroscopy. We find that ultrafast charge injection from the perovskite into the different HTMs (<100 fs) competes with carrier thermalization and occurs independently of their ionization energy. Our results prove that injection takes place from hot states in the valence band making this efficient even for HTMs with higher ionization energy than that of the perovskite. Moreover, a new trapping mechanism is observed after the addition of HTMs, which is attributed to interfacial electron traps formed between the $CH_3NH_3PbI_3$ and the HTMs, in addition to traps in the neat perovskite. Interfacial electron trapping is slower compared to the ultrafast hole injection, which contributes to the high efficiency obtained when these HTMs are employed in solar cells.

I. INTRODUCTION

Metal halide perovskites that have the general chemical formula ABX_3, where A is an inorganic or organic monovalent cation, B is a divalent metal cation, and X is a halogen atom, are proving themselves as efficient light-harvesters for solar cell applications.[1–3] Key benefits over other thin-film alternatives are their high absorption coefficient, low exciton binding energy, and long carrier diffusion lengths.[4] In addition, the versatility of the material allows modifications to form perovskites with higher exciton binding energies, tuneable bandgap, and narrow emission bandwidth for light-emitting diodes (LEDs).[5–7] Concerning perovskite solar cells (PSCs), the exceptionally steep increase in their performance within the last few years situates them amongst the most promising candidates to provide a solution for modern energetic demands, either in the single junction[8] or, as recently shown, in multijunction tandem devices.[9–11] Standard single junction devices consist of an absorber perovskite, such as $CH_3NH_3PbI_3$ (MAPI), interposed between an electron-transporting material (ETM) and a hole-transporting material (HTM).[12] In these devices, the favorable processes of charge formation and subsequent electron and hole extraction are in kinetic competition with undesirable processes, such as trapping, that can lead to recombination losses.[13] Therefore, the main role of the ETM and HTM layers is to facilitate the charge transport to the electrodes, block undesired back injection, and help the long-term stability of the PSCs.[14,15]

Characteristics that are typically taken into consideration for the choice of a HTM are the ionization energy (IE), the hole mobility, and the photochemical stability, as well as a suitable light absorption that does not interfere with the perovskite absorption when the HTM is on the side of light incidence.[16] Concerning the IE, a favorable offset with respect to the perovskite valence band (VB) is in theory necessary for an efficient hole injection. However, there are contradictory reports about the impact of the difference in IE

between the perovskite and HTM on the solar cell performance and V_{oc}. Recent experimental results, including on the systems investigated here, show that the use of HTMs with different IEs does not determine the device V_{oc} within the explored range.[17–20] Similarly, V_{oc} has been reported to be independent on the difference in the built-in potential, when employing ETMs with different work functions (WFs) in devices containing Spiro-OMeTAD as the HTM.[21]

Previous studies have highlighted the influence of trapping on the V_{oc} of PSCs.[22–25] This has been one of the main drives to understand the role of perovskite defects. Many studies have shown the defect-tolerance of MAPI concerning its intrinsic bulk defects,[26–30] and a lot of progress on the reduction intrinsic surface trap states has been made.[31–35] Additional surface states can be formed at the interface with an ETM or HTM, which can act as active interfacial traps if their energy lies in the bandgap. Along this line, an increased crystallinity of the MAPI perovskite can result in a V_{oc} enhancement, thus highlighting the effect of the trap states.[36]

Besides the influence of the trap states on V_{oc}, their impact on hole injection to an HTM remains uncertain. Moreover, the exact mechanism of the hole injection, in general, remains not very well understood. A broad range of time-constants for the hole injection has been reported, even when using the same HTM (Spiro-OMeTAD).[13,37–45] In particular, fast (80 fs up to 1 ps),[13,37–41] intermediate (8 ps),[42] and slow (0.75 ns to tens of nanosecond)[43–45] hole injection times have been reported for Spiro-OMeTAD. On the other hand, slow hole injection rates have been found for polymeric HTMs.[46] The dependence of the hole injection rate on the energetic alignment of the HTM IE with the perovskite VB is of high importance for the design rules of novel HTMs aiming to increase the efficiencies of PSCs.

In this context, we use femtosecond transient absorption (TA) spectroscopy to determine the injection dynamics between MAPI and organic HTMs with different IEs, as well as the interfacial trapping processes. This analysis helps to elucidate the main mechanism of hole injection, while highlighting the importance of the interfacial traps. The hole injection into the HTMs, the intrinsic electron trapping present in the neat perovskite, and the interfacial electron trapping upon the addition of the HTMs are studied. A relatively broad energetic distribution of traps is detected in neat MAPI. We then find that hole injection faster than 100 fs occurs independently of the IE of the HTM, while the electron trapping takes place at longer times. Finally, an additional mechanism due to interfacial trapping is revealed upon the addition of the HTMs in contact with the perovskite.

II. RESULTS AND DISCUSSION

Since up to now most of the research has focused on Spiro-OMeTAD, our study provides useful insights into the aforementioned processes for novel HTMs with different IEs and the additional benefit of being compatible with vacuum-deposition. Vacuum-depositing perovskites and HTMs without further post-treatment minimize the influence of the deposition conditions on the interface as it avoids solvent considerations. It is a well-established technique in the electronics industry and has proven to be very promising for large-scale commercialization of the PSCs.[47] The analyzed systems were chosen based on their good performance when employed in complete working solar cell devices, despite the different offset between the perovskite VB and the IE of the HTM.[19,20] The HTMs studied are 4,4′,4′′-Tris[phenyl(*m*-tolyl) amino]triphenylamine (*m*-MTDATA), N4,N4,N4”,N4”-tetra([1, 1′-biphenyl]-4-yl)-[1,1′:4′,1”-terphenyl]-4,4”-diamine (TaTm), and Tris(4-carbazoyl-9-ylphenyl)amine (TCTA). Their ionization energies were measured by Dänekamp *et al.* by photo-electron spectroscopy to be 5.0 eV, 5.4 eV, and 5.7 eV,[20] respectively, thus having a positive, a zero, or a negative offset with respect to the perovskite VB (5.4 eV), as shown in Fig. S1. The perovskite had the same thickness both in the neat film and the bilayers, while also the same thickness for the HTMs was used in all the bilayers. The thickness of the layers in the studied bilayers was measured by a profilometer and was found to be 250 nm for the perovskite and 100 nm for all the HTMs. More details on the sample preparation are given in the supplementary material, while the complete electrical characterization and the performance of the studied materials when employed in solar cell devices has been reported in our previous study.[20]

At first, we focus on the results for neat MAPI. We performed TA measurements on neat MAPI using excitation pulses at 600 nm and probing between 480 and 1100 nm. Measurements were carried out at a low pump fluence that corresponds to an initial photoexcited carrier density of 1.4×10^{17} cm^{-3}. Performing TA measurements at different excitation densities confirmed that no higher order recombination effects take place for this excitation density, as shown in Fig. S2. Figure 1(a) shows the TA spectra of neat MAPI at different time delays after excitation between 0.1 ps and 2 ns. The steady state photoluminescence (PL) spectrum is included in the same Figure.

A. TA on neat MAPI

The TA spectra of neat MAPI can be divided into spectral regions involving different processes. Figure 1(b) shows a simplified band diagram constructed according to a previous report.[48] In this band diagram, only the highest occupied VB and lowest unoccupied conduction band (CB) are included—necessary to describe our TA results—and the trap states probed from our TA measurements as discussed below. The transitions probed in the different spectral regions are also shown. More specifically, between 710 nm and 760 nm, depletion of the VB and filling of the CB are probed as a negative TA signal named visible ground state bleaching [vis GSB, orange arrow in Fig. 1(b)]. Upon ultrafast photoexcitation, band-filling competes with bandgap renormalization (BGR),[49,50] while after the first few picoseconds, most of carriers have relaxed to the CB and VB edges[51] and GSB recovery takes place due to carriers returning from the CB edge to the VB edge or relaxing to the trap states within the gap. The latter is evident by the broader GSB band during the first 100 fs and its narrowing at longer times. In the region between 500 nm and 710 nm, a visible photo-induced absorption (vis PIA) is attributed either to photo-induced refractive index changes[50] and/or to transitions of free carriers from the CB edge to higher states within the CB or higher CBs and/or from lower VB states or lower VBs to the VB edge [green arrow in Fig. 1(b)].

Moreover, we probed in the n-IR region between 850 nm and 1100 nm, which correspond to energies smaller than the bandgap.

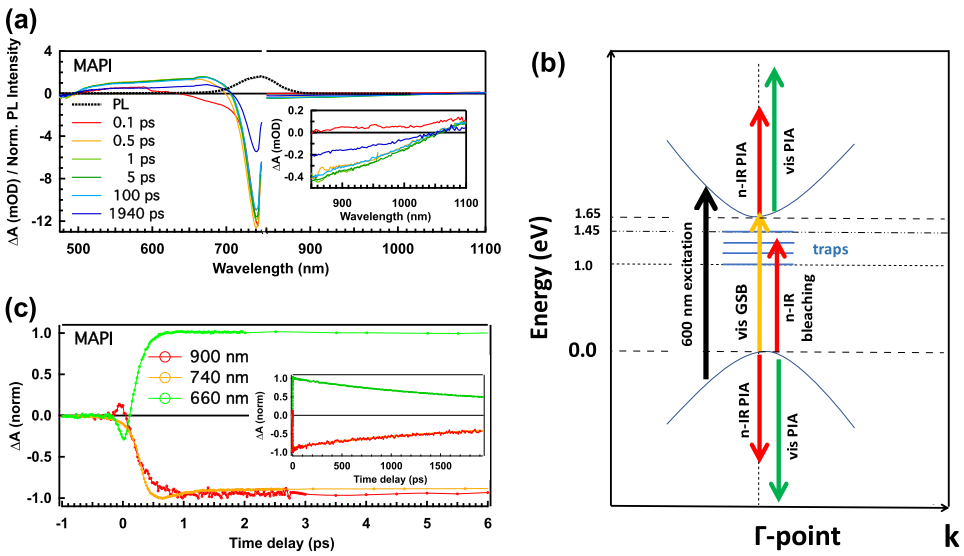

FIG. 1. (a) TA spectra at different time delays after 600 nm excitation and normalized PL spectrum (dotted black line) for neat MAPI. The inset shows a zoom on the n-IR spectral region. (b) A simplified band diagram for the Γ-valley in neat MAPI is shown that includes only the highest occupied valence band and lowest unoccupied conduction band. In addition, the trap levels probed via our TA measurements are included. With solid arrows, the transitions that are probed at different spectral regions are shown. (c) TA dynamics at short times after 600 nm excitation detected at different probed wavelengths for neat MAPI. The decays for the complete time-window are shown in the inset.

TA signals arising from three different origins are expected in this spectral region and are shown with red arrows in Fig. 1(b). First, intraband transitions within the CB result in a positive PIA (n-IR PIA). Second, intraband transitions within the same VB can also contribute to a positive PIA. Third, the presence of trap states located within the bandgap will result in a negative photo-bleaching signal (n-IR bleaching). At early times, we observe a small positive signal that disappears very quickly and becomes negative for longer times, as shown in Figs. 1(a) and 1(c). In order for the difference between the TA dynamics probed at the GSB and at 900 nm to be explained, the inclusion of trap states is necessary. In the absence of trap states that lead to the negative signal, only positive PIA should be evident in the n-IR region. By contrast, at times longer than 100 fs, the positive PIA is converted into a negative signal due to filling of the trap states, thus confirming their presence. The observation of the n-IR TA signal and its characteristics is in line with previous results,[39,52] which also associate them to the existence of trap states at the perovskite surface. Also, the PL spectrum of the neat perovskite studied here extends only up to 880 nm [Fig. 1(a)]; therefore, it cannot influence the signatures observed in the n-IR range. Due to the large width of the n-IR bleaching band, we conclude that a distribution of traps (1.180–1.458 eV, measured from the VB maximum) exists in the vacuum-deposited perovskite. This is in line with the results of several previous studies.[53–56] Their position in the bandgap coincides with the energy level of positive interstitial iodine predicted in a recent theoretical work,[30] which postulates the role of iodine interstitials as donor defects and thus as electron traps. The population of hole traps cannot be probed directly because it lies outside our detection window.

B. Hole injection in MAPI/HTM bilayers

To study the hole injection to the HTMs, we performed TA measurements on perovskite/HTM bilayers. The TA spectra at different time delays after excitation at 600 nm for the bilayer of MAPI with *m*-MTDATA are shown in Fig. 2(a), while the ones for the bilayers with TaTm and TCTA are shown in the supplementary material (Fig. S3). Using 600 nm as the excitation wavelength ensures that only the perovskite and not the HTM is excited, as confirmed by the steady state absorption spectra shown in Fig. S4. The HTMs studied here absorb at higher photon energies than the pump.

In Fig. 2(b), we compare the normalized TA dynamics detected at the vis GSB maximum in the bilayers with the different HTMs. As shown in the inset of Fig. 2(b), we observe a faster GSB decay, already from the first 100 fs onwards, upon the addition of the HTMs in contact with MAPI. This result combined with the smaller initial amplitude of the vis GSB seen for the bilayers [Fig. 2(c)] provides evidence that hole injection to the HTMs takes place at very fast time scales competing with our time resolution (≈80 fs). Indeed, since measurements for the perovskite and bilayers with HTMs were performed at the same absorbed excitation density (1.4×10^{17} cm^{-3}) for all cases, the smaller initial GSB in the bilayers is indicative of the presence of a smaller number of carriers already during the first 100 fs due to fast injection of holes into the HTMs. This is faster than the reported hot-hole cooling toward the VB edge.[51] This reduction in the GSB amplitude could, in principle, also originate from a change of the refractive index upon the addition of the HTMs. However, the HTMs are expected to have a refractive index of around ≈1.7,[57,58] in-between that of the air (≈1.0) and that of MAPI (higher than 2.4),[10,59] which should not significantly affect the reflectivity of the samples. The ultrafast hole injection also justifies the red-shift between the vis GSB of neat MAPI and the bilayers observed in Fig. 2(c). The initial band-filling that takes place upon photo-excitation due to the occupation of higher intra-band states leads to a blue-shift of the early GSB. Ultrafast hole injection in the bilayers implies that there are less holes available to occupy the states of the perovskite VB and to contribute to band-filling, leading to a smaller blue-shift of the initial vis GSB (it is more red-shifted with respect to the neat MAPI film).

A rise of the polaron signal from the HTM occurring on the same time scale as the observed reduction in the perovskite GSB

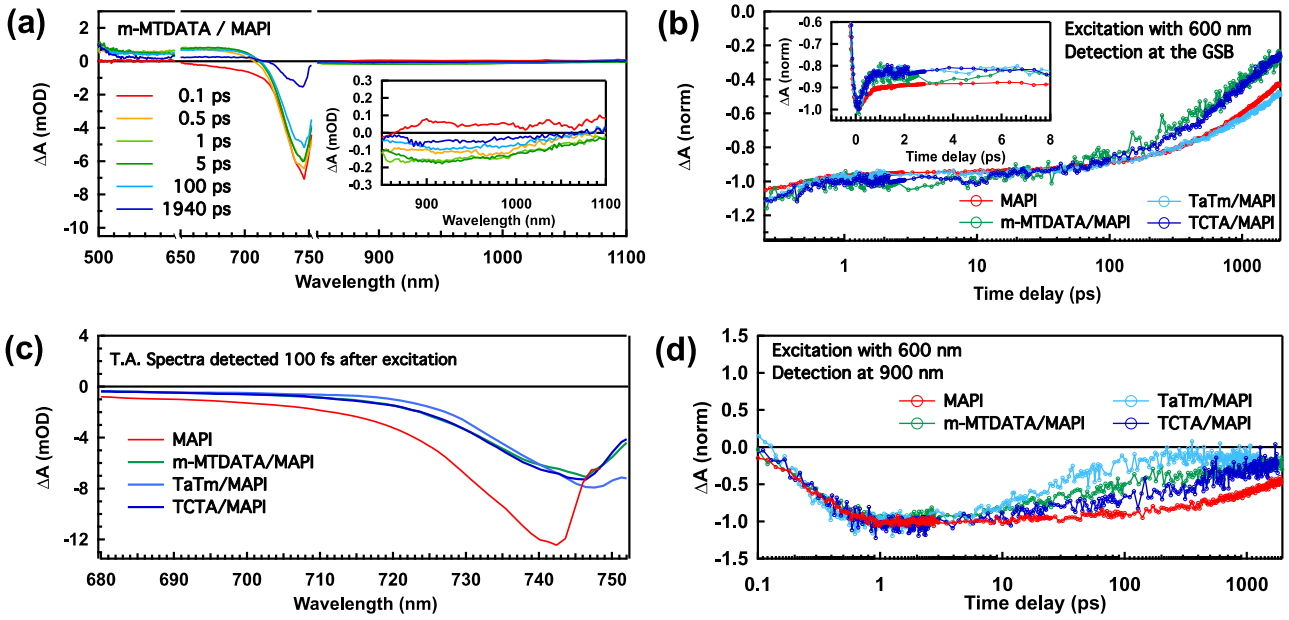

FIG. 2. (a) TA spectra at different time-delays for the *m*-MTDATA/MAPI bilayer following excitation at 600 nm. (b) TA dynamics normalized at 0.75 ps, detected at the respective vis GSB band maximum of neat MAPI and *m*-MTDATA/MAPI, TaTm/MAPI and TCTA/MAPI bilayers. The inset shows the early time dynamics normalized at 0 ps. (c) TA spectra of neat MAPI and MAPI/HTM films detected 100 fs after excitation. (d) Normalized TA dynamics detected at 900 nm for all studied systems.

would be an absolute proof for the occurrence of hole injection. However in our case, the TA spectra of MAPI/m-MTDATA, as well as the other HTMs, show comparable signatures in the visible range with neat MAPI and the oxidized state of the HTMs is not observed. This is because the signature of the oxidized state of the HTMs is not accessible in our experiment since it is expected to lie further in the IR or to overlap with the signatures of the perovskite in the visible range, as has been previously reported.[37,39] Some differences are nevertheless observed in the n-IR range [inset of Fig. 2(a)] and will be discussed below.

Figure 2(d) shows the normalized TA dynamics of all samples detected at 900 nm, where the trap population is probed. Since the same rise time of the negative n-IR bleaching signal at 900 nm in the neat perovskite and bilayer systems is observed, we exclude that the ultrafast initial decay seen for the vis GSB in the bilayers arises from filling of the traps (and confirm its origin due to hole injection). However, the difference in the dynamics between the perovskite and the bilayers seen after the first 10 ps will be explained below in terms of interfacial trapping.

The observed ultrafast hole injection for all HTMs, independently of their favorable or unfavorable IE, is in line with previous reports on the hole injection from MAPI to Spiro-OMeTAD,[13,37–41] NiO_x,[60] vacancy-engineered MoS_2,[61] poly(triarylamine) (PTAA), and poly(3,4-ethylenedioxythiophene):poly(styrene sulfonate) (PEDOT:PSS).[62] The efficient hole injection is further confirmed by the fact that solar cell devices employing all the studied HTMs are functional[20] and is in line with previous reports on the independence of V_{oc} on the IE of the HTM.[36,63] However, we cannot exclude any nanosecond hole transfer, as has been reported for both Spiro-OMeTAD[43–45] and different polymeric HTMs such as PTAA, poly(3-hexylthiophee-2,5-diyl) (P3HT), and poly[2,6-(4,4-bis(2-ethylhexyl)-4Hcyclopenta[2,1-b; 3,4-b′]dithiophene)-alt-4,7-(2,1,3-benzothiadiazole)] (PCPDTBT),[46] since this is outside of the studied time window.

As already mentioned above, the hole injection in the bilayers competes with carrier thermalization processes such as band-filling and bandgap renormalization. This is evident in Fig. S5, where the dynamics detected at a short and a long wavelength of the vis GSB band for neat MAPI and the *m*-MTDATA/MAPI bilayer are compared. The dynamics detected at the short wavelength is faster than the one detected at the longer wavelength in both the neat perovskite and the perovskite/HTM bilayers. The longer rise time at the longer wavelength is due to the time that the carriers need to relax form higher states to the band-edge. The decay at the short wavelength is faster for the bilayer because of the loss of the carriers due to the fast hole injection toward the HTM and thus less carriers will thermalize to the band edge of the perovskite. This clearly shows that the hole injection to the HTM is faster than the thermalization. Eventually, less carriers will thermalize to the band edge of the perovskite in the bilayers and therefore the relaxation to the band edge in the bilayers is faster compared to that seen for the neat MAPI.

The differences in the relaxation times to the band edge, the smaller amplitude of the initial GSB, and the red-shifted GSB support our conclusion for ultrafast charge transfer from the perovskite to the studied HTMs. The observation of ultrafast hole injection, further supported by the efficient charge extraction in solar cell devices made with all HTMs,[20] is particularly significant for the case of TCTA, where hole injection should not be expected judging from the negative offset between the VB of the perovskite and the IE of the HTM. As was shown above, the hole injection competes with the

processes of band-filling and bandgap renormalization; therefore, it is possible that the hole injection does not take place from the VB edge but from hot states which lie deeper in the VB. In this case, the energetic off-set allows the process to take place.

C. Interfacial electron trapping in perovskite/HTM bilayers

Differences between TA results in neat MAPI and the perovskite/HTM bilayers can be used to draw conclusions regarding the electron trapping and recombination processes in these systems. As mentioned above, the dynamics of the MAPI bilayers with HTMs detected in the n-IR bleaching band at 900 nm [Fig. 2(d)] are faster compared to neat MAPI at times longer than 10 ps. Moreover, looking at the TA spectra of neat MAPI [Fig. 1(a)] and the bilayers of *m*-MTDATA and TaTm [Figs. 2(a) and S3], a different n-IR bleaching band shape is observed upon the addition of the HTMs, indicating in part a different origin of this band. For the case of TCTA, there is not an obvious spectral change and differences can be obtained from the analysis of the dynamics provided below.

To further analyze our results and to clarify the differences in the relaxation/recombination processes between the studied systems, we used global analysis on our TA results. This procedure is useful for the disentanglement of trapping processes at intrinsic perovskite traps and interfacial trapping present upon the addition of the different HTMs. The entire TA datasets at all times after the pulse rise are simultaneously fitted to obtain the relaxation mechanisms and the respective time constants related to each process. Since an *a priori* kinetic model is missing, the data are simulated by a sum of exponential decays along with their amplitudes, as shown in Eq. (1),

$$\Delta A = \sum_{i=1}^{2,3} A_i \cdot e^{-\frac{t}{\tau_i}}, \quad (1)$$

where A_i is the amplitude and τ_i is the corresponding time constant of each relaxation/recombination mechanism. A certain time constant is attributed to a relaxation amplitude that corresponds to the fraction of the TA signal that participates in this relaxation process over the whole detection range. Plotting the amplitudes vs the probed wavelengths, the decay associated spectra (DAS) are obtained. Here, the DAS of neat MAPI, *m*-MTDATA/MAPI, TaTm/MAPI, and TCTA/MAPI are shown in Figs. 3(a)–3(d). Due to our time window that does not exceed 2 ns, we cannot define with accuracy the long-lived component. The value given in the global analysis is a minimum limit, especially in the case of neat perovskite, where a higher PB signal is still present at long times.

For the neat perovskite, the inclusion of only two relaxation/recombination mechanisms was sufficient to analyze the data in agreement with previous reports.[43] The ultrafast time constant (τ_1 = 366 fs) corresponds to the relaxation of the carriers to the band-edges,[50,51,64,65] while τ_2 = 1.4 ns represents the processes that contribute to ground state recovery, namely, band-to-band recombination and trapping. By contrast, the inclusion of an additional relaxation/recombination mechanism with a time-constant of tens of ps was necessary for all perovskite/HTM bilayers. The additional mechanism is attributed to the existence of an interfacial process different from the intrinsic trapping recombination seen in neat MAPI. Therefore, we assign this new mechanism to interfacial electron trapping at the MAPI/HTM interface. Carriers in the perovskite recombine from these trap states with a time constant of tens of picosecond.

Additional trapping mechanisms upon the addition of the HTMs must be invoked to explain the trends observed in the

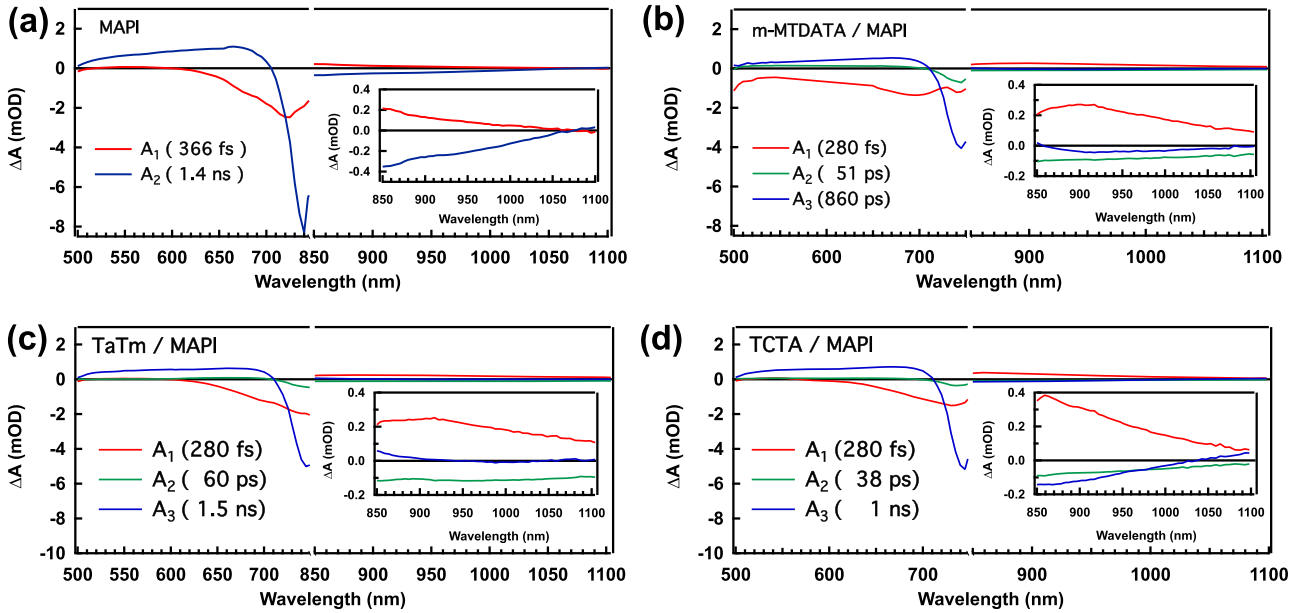

FIG. 3. Decay associated spectra related to the time constants obtained from the global analysis procedure for (a) neat MAPI, (b) *m*-TDATA/MAPI, (c) TaTm/MAPI, and (d) TCTA/MAPI.

dynamics detected at the vis GSB and at 900 nm in the bilayers [Figs. 2(b) and 2(d)], which contrast with the behavior seen in the neat perovskite [Fig. 1(c)]. The dynamics detected at the vis GSB at times longer than the ultrafast hole injection [Fig. 2(b)] is expected to be slower for the bilayers compared to the neat perovskite due to a smaller probability of the electrons to recombine with holes in the VB. This arises from the larger population of electrons in the CB compared to the population of holes in the VB, after the ultrafast hole injection. The slower recombination is however observed only for TaTm, while the rest of the bilayers show the opposite trend. This behavior can be explained by increased additional trapping in deeper interfacial states—not directly probed here—in TCTA/MAPI and *m*-MTDATA/MAPI that causes a reduction in the population of electrons in the CB, which results in the faster decay of the vis GSB compared to the neat perovskite. This observation suggests that interfacial recombination mechanisms are more important in the case of *m*-MDTATA and TCTA. This is in agreement with our previous results on solar cells with these HTMs,[20] where the higher V_{oc} in devices with TaTm as the HTM was attributed to dominant bulk trap-assisted recombination, in contrast to *m*-MTDATA and TCTA that showed enhanced surface recombination. The faster decay at 900 nm n-IR bleaching in the TaTm bilayer compared to the other ones [Fig. 2(d)] does not agree with the differences observed in the dynamics detected at the vis GSB [Fig. 2(b)] likely because the overall recombination should also include hole trapping, which is not directly accessed in our measurements.

The nature of the surface states in neat MAPI is expected to be the same as the one in the bulk, attributed to iodine interstitials that can act as electron or hole traps due to their amphotericity.[30] The new interfacial trapping channel observed upon the addition of the HTMs could originate from the same iodine interstitials that are present in the bulk (donor I^+ acting as electron traps) but at a higher density, thus manifesting themselves stronger in the TA data.

As both the decay constant τ_2 and its amplitude A_2, related to the interfacial trapping, are comparable for all the HTMs (Fig. 3), the electron trapping is not expected to be responsible for the changes seen in V_{oc}. It has indeed been shown that hole traps will play a more crucial role in the recombination, as concluded from the full device analysis.[20] Therefore, despite the interfacial electron trapping channel that we evidence here, all devices have a good efficiency. This can be explained by the ultrafast hole injection, which is significantly faster than the interfacial electron trapping, in combination with the low density of traps as seen from the low TA amplitude of the n-IR bleaching compared to the vis GSB. Finally, it should be mentioned that we cannot exclude the existence of electron trapping on time scales exceeding our time window, as reported previously.[66,67,55]

III. CONCLUSIONS

In summary, the dynamics of hole injection and interfacial trapping of electrons in bilayers of the MAPI perovskite with hole transporting materials of different ionization energies were studied. Our results indicate that hole injection to the different HTMs takes place within 100 fs following photo-excitation. More interestingly, for the studied range, the hole injection is found to take place independently of the ionization energy offset with respect to the perovskite valence band (from >300 meV to <−300 meV). We explain that this is because hole injection can occur even from hot states since it occurs very fast on a time that competes with carrier thermalization. This finding releases constraints on energy level considerations when looking for novel HTMs and shifts the focus on other properties such as the conductivity of the HTMs which can improve the fill factor of the devices. Concerning traps, we find a broad distribution of donor states, acting as electron traps, located within the energy bandgap of the perovskite for both the neat perovskite and the bilayers. We reveal an additional trapping mechanism in the bilayers due to interfacial trapping of electrons. The similar amplitude and time constant measured for the interfacial trapping mechanism shows that its effect is similar in all the studied HTM bilayers. Also, the interfacial electron trapping is much slower compared to the hole injection. Thus, electron trap states are not expected to influence significantly V_{oc} and efficiency of PSCs.

SUPPLEMENTARY MATERIAL

See supplementary material for information on the sample preparation, energy diagram showing the offset between the MAPI VB and the IE of the different HTMs, experimental setup, and conditions for femtosecond transient absorption spectroscopy, excitation density dependent measurements on the neat MAPI film, TA spectra of the TaTm/MAPI and TCTA/MAPI bilayers, steady state absorption spectra of all the samples, comparison between the dynamics of the neat MAPI, and the *m*-MTDATA/MAPI bilayer at two different detection wavelengths in the GSB band.

ACKNOWLEDGMENTS

We acknowledge financial support from the European Union H2020 project INFORM (Grant No. 675867). N.D., D.T., and N.B. would like to acknowledge the University of Bern, Switzerland, for providing funding and infrastructure. Financial support is acknowledged from the Spanish Ministry of Economy and Competitiveness (MINECO) via the Unidad de Excelencia María de Maeztu Grant Nos. MDM-2015-0538 and MAT2017-88821-R and the Generalitat Valenciana (Grant No. Prometeo/2016/135). P.P.B. thanks the MINECO for his RyC contract and acknowledges the financial support from the Conselleria d'Educació, Investigació, Cultura i Esport Valenciana (Grant No. SEJI2017/2017/012).

REFERENCES

[1] A. Kojima, K. Teshima, Y. Shirai, and M. Tsutomu, "Organometal halide perovskites as visible-light sensitizers for photovoltaic cells," J. Am. Chem. Soc. **131**, 6050–6051 (2009).

[2] M. M. Lee, J. Teuscher, T. Miyasaka, T. N. Murakami, and H. J. Snaith, "Efficient hybrid solar cells based on meso-superstructured organometal halide perovskites," Science **338**, 643–647 (2012).

[3] H.-S. Kim, C.-R. Lee, J.-H. Im, K.-B. Lee, T. Moehl, A. Marchioro, S.-J. Moon, R. Humphry-Baker, J.-H. Yum, J. E. Moser *et al.*, "Lead iodide perovskite sensitized all-solid-state submicron thin film mesoscopic solar cell with efficiency exceeding 9%," Sci. Rep. **2**, 591 (2012).

[4] J. Huang, Y. Yuan, Y. Shao, and Y. Yan, "Understanding the physical properties of hybrid perovskites for photovoltaic applications," Nat. Rev. Mater. **2**, 17042 (2017).

[5]N. Yantara, S. Bhaumik, F. Yan, D. Sabba, H. A. Dewi, N. Mathews, P. P. Boix, H. V. Demir, and S. Mhaisalkar, "Inorganic halide perovskites for efficient light-emitting diodes," J. Phys. Chem. Lett. **6**, 4360–4364 (2015).
[6]S. D. Stranks and H. J. Snaith, "Metal-halide perovskites for photovoltaic and light-emitting devices," Nat. Nanotechnol. **10**, 391–402 (2015).
[7]B. R. Sutherland and E. H. Sargent, "Perovskite photonic sources," Nat. Photonics **10**, 295–302 (2016).
[8]S. Kazim, M. K. Nazeeruddin, M. Grätzel, and S. Ahmad, "Perovskite as light harvester: A game changer in photovoltaics," Angew. Chem., Int. Ed. **53**, 2812–2824 (2014).
[9]H. Shen, T. Duong, Y. Wu, J. Peng, D. Jacobs, N. Wu, K. Weber, T. White, and K. Catchpole, "Metal halide perovskite: A game-changer for photovoltaics and solar devices via a tandem design," Sci. Technol. Adv. Mater. **19**, 53–75 (2018).
[10]J. Ávila, C. Momblona, P. Boix, M. Sessolo, M. Anaya, G. Lozano, K. Vandewal, H. Míguez, and H. J. Bolink, "High voltage vacuum-deposited $CH_3NH_3PbI_3$–$CH_3NH_3PbI_3$ tandem solar cells," Energy Environ. Sci. **11**, 3292–3297 (2018).
[11]F. Sahli, J. Werner, B. A. Kamino, M. Bräuninger, R. Monnard, B. Paviet-Salomon, L. Barraud, L. Ding, J. J. Diaz Leon, D. Sacchetto *et al.*, "Fully textured monolithic perovskite/silicon tandem solar cells with 25.2% power conversion efficiency," Nat. Mater. **17**, 820–826 (2018).
[12]J. P. C. Baena, L. Steier, W. Tress, M. Saliba, S. Neutzner, T. Matsui, F. Giordano, T. J. Jacobsson, A. R. S. Kandada, S. M. Zakeeruddin *et al.*, "Highly efficient planar perovskite solar cells through band alignment engineering," Energy Environ. Sci. **8**, 2928–2934 (2015).
[13]A. Marchioro, J. Teuscher, D. Friedrich, M. Kunst, R. van de Krol, T. Moehl, M. Grätzel, and J.-E. Moser, "Unravelling the mechanism of photoinduced charge transfer processes in lead iodide perovskite solar cells," Nat. Photonics **8**, 250 (2014).
[14]M. Liu, M. B. Johnston, and H. J. Snaith, "Efficient planar heterojunction perovskite solar cells by vapour deposition," Nature **501**, 395 (2013).
[15]B. Roose, Q. Wang, and A. Abate, "The role of charge selective contacts in perovskite solar cell stability," Adv. Energy Mater. **9**, 1803140 (2018).
[16]X. Zhao and M. Wang, "Organic hole-transporting materials for efficient perovskite solar cells," Mater. Today Energy **7**, 208–220 (2018).
[17]R. A. Belisle, P. Jain, R. Prasanna, T. Leijtens, and M. D. McGehee, "Minimal effect of the hole-transport material ionization potential on the open-circuit voltage of perovskite solar cells," ACS Energy Lett. **1**, 556–560 (2016).
[18]J. Zhang, B. Xu, M. B. Johansson, N. Vlachopoulos, G. Boschloo, L. Sun, E. M. J. Johansson, and A. Hagfeldt, "Strategy to boost the efficiency of mixed-ion perovskite solar cells: Changing geometry of the hole transporting material," ACS Nano **10**, 6816–6825 (2016).
[19]D. Pérez-Del-Rey, P. P. Boix, M. Sessolo, A. Hadipour, and H. J. Bolink, "Interfacial modification for high-efficiency vapor-phase-deposited perovskite solar cells based on a metal oxide buffer layer," J. Phys. Chem. Lett. **9**, 1041–1046 (2018).
[20]B. Dänekamp, N. Droseros, D. Tsokkou, V. Brehm, P. P. Boix, M. Sessolo, N. Banerji, and H. J. Bolink, "Influence of hole transport material ionization energy on the performance of perovskite solar cells," J. Mater. Chem. C **7**, 523–527 (2019).
[21]S. Ravishankar, S. Gharibzadeh, C. Roldán-Carmona, G. Grancini, Y. Lee, M. Ralaiarisoa, A. M. Asiri, N. Koch, J. Bisquert, and M. K. Nazeeruddin, "Influence of charge transport layers on open-circuit voltage and hysteresis in perovskite solar cells," Joule **2**, 788–798 (2018).
[22]W. Tress, "Perovskite solar cells on the way to their radiative efficiency limit—Insights into a success story of high open-circuit voltage and low recombination," Adv. Energy Mater. **7**, 1602358 (2017).
[23]J.-P. Correa-Baena, M. Anaya, G. Lozano, W. Tress, K. Domanski, M. Saliba, T. Matsui, T. J. Jacobsson, M. E. Calvo, A. Abate *et al.*, "Unbroken perovskite: Interplay of morphology, electro-optical properties, and ionic movement," Adv. Mater. **28**, 5031–5037 (2016).
[24]J.-P. Correa-Baena, W. Tress, K. Domanski, E. H. Anaraki, S.-H. Turren-Cruz, B. Roose, P. P. Boix, M. Grätzel, M. Saliba, A. Abate *et al.*, "Identifying and suppressing interfacial recombination to achieve high open-circuit voltage in perovskite solar cells," Energy Environ. Sci. **10**, 1207–1212 (2017).
[25]W. Tress, M. Yavari, K. Domanski, P. Yadav, B. Niesen, J. P. Correa Baena, A. Hagfeldt, and M. Graetzel, "Interpretation and evolution of open-circuit voltage, recombination, ideality factor and subgap defect states during reversible light-soaking and irreversible degradation of perovskite solar cells," Energy Environ. Sci. **11**, 151–165 (2018).
[26]J. L. Miller, "Unusual defect physics underlies perovskite solar cells' exceptional performance," Phys. Today **67**(5), 13–15 (2014).
[27]A. Buin, R. Comin, J. Xu, A. H. Ip, and E. H. Sargent, "Halide-dependent electronic structure of organolead perovskite materials," Chem. Mater. **27**, 4405–4412 (2015).
[28]M. L. Agiorgousis, Y. Y. Sun, H. Zeng, and S. Zhang, "Strong covalency-induced recombination centers in perovskite solar cell material $CH_3NH_3PbI_3$," J. Am. Chem. Soc. **136**, 14570–14575 (2014).
[29]A. Walsh, D. O. Scanlon, S. Chen, X. G. Gong, and S. H. Wei, "Self-regulation mechanism for charged point defects in hybrid halide perovskites," Angew. Chem., Int. Ed. **54**, 1791–1794 (2015).
[30]D. Meggiolaro, S. Motti, E. Mosconi, A. barker, J. Ball, C. A. R. Perini, F. Deschler, A. Petrozza, and F. De Angelis, "Iodine chemistry determines the defect tolerance of lead-halide perovskites," Energy Environ. Sci. **11**, 702–713 (2018).
[31]M. Yuan, L. N. Quan, R. Comin, G. Walters, R. Sabatini, O. Voznyy, S. Hoogland, Y. Zhao, E. M. Beauregard, P. Kanjanaboos *et al.*, "Perovskite energy funnels for efficient light-emitting diodes," Nat. Nanotechnol. **11**, 872–877 (2016).
[32]Y. Tian, C. Zhou, M. Worku, X. Wang, Y. Ling, H. Gao, Y. Zhou, Y. Miao, J. Guan, and B. Ma, "Highly efficient spectrally stable red perovskite light-emitting diodes," Adv. Mater. **30**, 1707093 (2018).
[33]J. Wang, N. Wang, Y. Jin, J. Si, Z.-K. Tan, H. Du, L. Cheng, X. Dai, S. Bai, H. He *et al.*, "Interfacial control toward efficient and low-voltage perovskite light-emitting diodes," Adv. Mater. **27**, 2311–2316 (2015).
[34]S. Ham, Y. J. Choi, J. W. Lee, N. G. Park, and D. Kim, "Impact of excess CH_3NH_3I on free carrier dynamics in high-performance nonstoichiometric perovskites," J. Phys. Chem. C **121**, 3143–3148 (2017).
[35]B. Dänekamp, N. Droseros, F. Palazon, M. Sessolo, N. Banerji, and H. J. Bolink, "Efficient photo-and electroluminescence by trap states passivation in vacuum-deposited hybrid perovskite thin films," ACS Appl. Mater. Interfaces **10**, 36187–36193 (2018).
[36]T. Du, J. Kim, J. Ngiam, S. Xu, P. R. F. Barnes, J. R. Durrant, and M. A. McLachlan, "Elucidating the origins of subgap tail states and open-circuit voltage in methylammonium lead triiodide perovskite solar cells," Adv. Funct. Mater. **28**, 1801808 (2018).
[37]J. C. Brauer, Y. H. Lee, K. N. Mohammad, and N. Banerji, "Ultrafast charge carrier dynamics in $CH_3NH_3PbI_3$: Evidence for hot hole injection into spiro-OMeTAD," J. Mater. Chem. C **4**, 5922 (2016).
[38]P. Piatkowski, B. Cohen, F. Javier Ramos, M. Di Nunzio, M. K. Nazeeruddin, M. Grätzel, S. Ahmad, and A. Douhal, "Direct monitoring of ultrafast electron and hole dynamics in perovskite solar cells," Phys. Chem. Chem. Phys. **17**, 14674–14684 (2015).
[39]G. Grancini, D. Viola, Y. Lee, M. Saliba, S. Paek, K. T. Cho, S. Orlandi, M. Cavazzini, F. Fungo, M. I. Hossain *et al.*, "Femtosecond charge-injection dynamics at hybrid perovskite interfaces," ChemPhysChem **18**, 2381–2389 (2017).
[40]C. S. Ponseca, E. M. Hutter, P. Piatkowski, B. Cohen, T. Pascher, A. Douhal, A. Yartsev, V. Sundström, and T. J. Savenije, "Mechanism of charge transfer and recombination dynamics in organo metal halide perovskites and organic electrodes, PCBM, and spiro-OMeTAD: Role of dark carriers," J. Am. Chem. Soc. **137**, 16043–16048 (2015).
[41]H.-J. Yan, Z.-L. Ku, X.-F. Hu, W.-Y. Zhao, M.-J. Zhong, Q.-B. Zhu, X. Lin, Z.-M. Jin, and G.-H. Ma, "Ultrafast terahertz probes of charge transfer and recombination pathway of $CH_3NH_3PbI_3$ perovskites," Chin. Phys. Lett. **35**, 028401 (2018).
[42]J. Leng, J. Liu, J. Zhang, and S. Jin, "Decoupling interfacial charge transfer from bulk diffusion unravels its intrinsic role for efficient charge extraction in perovskite solar cells," J. Phys. Chem. Lett. **7**, 5056–5061 (2016).
[43]K. Pydzińska, J. Karolczak, I. Kosta, R. Tena-Zaera, A. Todinova, J. Idígoras, J. A. Anta, and M. Ziółek, "Determination of interfacial charge-transfer rate constants in perovskite solar cells," ChemSusChem **9**, 1647–1659 (2016).

[44]G. Xing, N. Mathews, S. Sun, S. S. Lim, Y. M. Lam, M. Grätzel, S. Mhaisalkar, and T. C. Sum, "Long-range balanced electron- and hole-transport lengths in organic-inorganic $CH_3NH_3PbI_3$," Science **342**, 344–347 (2013).
[45]E. M. Hutter, J.-J. Hofman, M. L. Petrus, M. Moes, R. D. Abellón, P. Docampo, and T. J. Savenije, "Charge transfer from methylammonium lead iodide perovskite to organic transport materials: Efficiencies, transfer rates, and interfacial recombination," Adv. Energy Mater. **7**, 1602349 (2017).
[46]J. C. Brauer, Y. H. Lee, M. K. Nazeeruddin, and N. Banerji, "Charge transfer dynamics from organometal halide perovskite to polymeric hole transport materials in hybrid solar cells," J. Phys. Chem. Lett. **6**, 3675–3681 (2015).
[47]C. Momblona, L. Gil-Escrig, E. Bandiello, E. M. Hutter, M. Sessolo, K. Lederer, J. Blochwitz-Nimoth, and H. J. Bolink, "Efficient vacuum deposited P-I-N and N-I-P perovskite solar cells employing doped charge transport layers," Energy Environ. Sci. **9**, 3456–3463 (2016).
[48]R. A. Jishi, O. B. Ta, and A. A. Sharif, "Modeling of lead halide perovskites for photovoltaic applications," J. Phys. Chem. C **118**, 28344–28349 (2014).
[49]J. S. Manser and P. V. Kamat, "Band filling with free charge carriers in organometal halide perovskites," Nat. Photonics **8**, 737–743 (2014).
[50]M. B. Price, J. Butkus, T. C. Jellicoe, A. Sadhanala, A. Briane, J. E. Halpert, K. Broch, J. M. Hodgkiss, R. H. Friend, and F. Deschler, "Hot carrier cooling and photoinduced refractive index changes in organic-inorganic lead halide perovskites," Nat. Commun. **6**, 8420 (2015).
[51]G. J. Hedley, C. Quarti, J. Harwell, O. V. Prezhdo, D. Beljonne, and I. D. W. Samuel, "Hot-hole cooling controls the initial ultrafast relaxation in methylammonium lead iodide perovskite," Sci. Rep. **8**, 8115 (2018).
[52]X. Wu, M. T. Trinh, D. Niesner, H. Zhu, Z. Norman, J. S. Owen, O. Yaffe, B. J. Kudisch, and X. Y. Zhu, "Trap states in lead iodide perovskites," J. Am. Chem. Soc. **137**, 2089–2096 (2015).
[53]A. Baumann, S. Väth, P. Rieder, M. C. Heiber, K. Tvingstedt, and V. Dyakonov, "Identification of trap states in perovskite solar cells," J. Phys. Chem. Lett. **6**, 2350–2354 (2015).
[54]A. D. Wright, R. L. Milot, G. E. Eperon, H. J. Snaith, M. B. Johnston, and L. M. Herz, "Band-tail recombination in hybrid lead iodide perovskite," Adv. Funct. Mater. **27**, 1700860 (2017).
[55]T. Leijtens, G. E. Eperon, A. J. Barker, G. Grancini, W. Zhang, J. M. Ball, A. R. S. Kandada, H. J. Snaith, and A. Petrozza, "Carrier trapping and recombination: The role of defect physics in enhancing the open circuit voltage of metal halide perovskite solar cells," Energy Environ. Sci. **9**, 3472–3481 (2016).
[56]V. Adinolfi, M. Yuan, R. Comin, E. S. Thibau, D. Shi, M. I. Saidaminov, P. Kanjanaboos, D. Kopilovic, S. Hoogland, Z.-H. Lu *et al.*, "The in-gap electronic state spectrum of methylammonium lead iodide single-crystal perovskites," Adv. Mater. **28**, 3406–3410 (2016).
[57]See https://www.chembk.com/en/chem/M-MTDATA for ChemBK. M-MT DATA, CAS 124729-98-2.
[58]See https://www.chembk.com/en/chem/TcTa for ChemBK. TCTA, CAS 139092-78-7.
[59]L. J. Phillips, A. M. Rashed, R. E. Treharne, J. Kay, P. Yates, I. Z. Mitrovic, A. Weerakkody, S. Hall, and K. Durose, "Maximizing the optical performance of planar $CH_3NH_3PbI_3$ hybrid perovskite heterojunction stacks," Sol. Energy Mater. Sol. Cells **147**, 327–333 (2016).
[60]A. Corani, M.-H. Li, P.-S. Shen, P. Chen, T.-F. Guo, A. El Nahhas, K. Zheng, A. Yartsev, V. Sundström, and C. S. Ponseca, "Ultrafast dynamics of hole injection and recombination in organometal halide perovskite using nickel oxide as P-type contact electrode," J. Phys. Chem. Lett. **7**, 1096–1101 (2016).
[61]B. Peng, G. Yu, Y. Zhao, Q. Xu, G. Xing, X. Liu, D. Fu, B. Liu, J. R. S. Tan, W. Tang *et al.*, "Achieving ultrafast hole transfer at the monolayer $MoS_2$and $CH_3NH_3PbI_3$ Perovskite interface by defect engineering," ACS Nano **10**, 6383–6391 (2016).
[62]K. Ishioka, B. G. Barker, M. Yanagida, Y. Shirai, and K. Miyano, "Direct observation of ultrafast hole injection from lead halide perovskite by differential transient transmission spectroscopy," J. Phys. Chem. Lett. **8**, 3902–3907 (2017).
[63]W. Yu, S. Yu, J. Zhang, W. Liang, X. Wang, X. Guo, and C. Li, "Two-in-one additive-engineering strategy for improved air stability of planar perovskite solar cells," Nano Energy **45**, 229–235 (2018).
[64]H.-Y. Hsu, C.-Y. Wang, A. Fathi, J.-W. Shiu, C.-C. Chung, P.-S. Shen, T.-F. Guo, P. Chen, Y.-P. Lee, and E. W.-G. Diau, "Femtosecond excitonic relaxation dynamics of perovskite on mesoporous films of Al_2O_3 and NiO nanoparticles," Angew. Chem. **126**, 9493–9496 (2014).
[65]K. Chen, A. J. Barker, F. L. C. Morgan, J. E. Halpert, and J. M. Hodgkiss, "Effect of carrier thermalization dynamics on light emission and amplification in organometal halide perovskites," J. Phys. Chem. Lett. **6**, 153–158 (2015).
[66]S. D. Stranks, V. M. Burlakov, T. Leijtens, J. M. Ball, A. Goriely, and H. J. Snaith, "Recombination kinetics in organic-inorganic perovskites: Excitons, free charge, and subgap states," Phys. Rev. Appl. **2**, 034007 (2014).
[67]Y. Yamada, T. Nakamura, M. Endo, A. Wakamiya, and Y. Kanemitsu, "Photocarrier recombination dynamics in perovskite $CH_3NH_3PbI_3$ for solar cell applications," J. Am. Chem. Soc. **136**, 11610–11613 (2014).